PAPER

3D bioprinting of mature bacterial biofilms for antimicrobial resistance drug testing

Evita Ning[1,5], Gareth Turnbull[2,3,5], Jon Clarke[3], Fred Picard[2,3], Philip Riches[2], Marc Vendrell[4], Duncan Graham[1], Alastair W Wark[1], Karen Faulds[1] and Wenmiao Shu[3]

[1] Centre for Molecular Nanometrology, Department of Pure and Applied Chemistry, Technology and Innovation Centre, University of Strathclyde, 99 George Street, Glasgow, G1 1RD, United Kingdom
[2] Department of Biomedical Engineering, University of Strathclyde, 50 George Street, Glasgow, G1 1QE, United Kingdom
[3] Department of Orthopaedics, Golden Jubilee National Hospital, Agamemnon Street, Clydebank, G81 4DY, United Kingdom
[4] Medical Research Council Centre for Inflammation Research, The University of Edinburgh, United Kingdom
[5] Both authors contributed equally to this work.
 Data associated with this publication, are openly available from the University of Strathclyde Knowledge Base at https://doi.org/10.15129/c86d843d-1e2d-4ba9-9905-06ab4dbc90a1

E-mail: will.shu@strath.ac.uk and karen.faulds@strath.ac.uk

Keywords: 3D bioprinting, biofilm, antimicrobial resistance, drug testing

Supplementary material for this article is available online

Abstract

The potential to bioprint and study 3D bacterial biofilm constructs could have great clinical significance at a time when antimicrobial resistance is rising to dangerously high levels worldwide. In this study, clinically relevant bacterial species including *Escherichia coli, Staphylococcus aureus* (MSSA), Methicillin-resistant *Staphylococcus aureus* (MRSA) and *Pseudomonas aeruginosa* were 3D bioprinted using a double-crosslinked alginate bioink to form mature bacteria biofilms, characterized by confocal laser scanning microscopy (CLSM) and fluorescent staining. Solid and porous bacteria-laden constructs were reproducibly bioprinted with thicknesses ranging from 0.25 to 4 mm. We demonstrated 3D bioprinting of thicker biofilms (>4 mm) than found in currently available *in vitro* models. Bacterial viability was excellent in the bioprinted constructs, with CLSM observation of bacterial biofilm production and maturation possible for at least 28 d in culture. Importantly, we observed the complete five-step biofilm life cycle *in vitro* following 3D bioprinting for the first time, suggesting the formation of mature 3D bioprinted biofilms. Bacterial growth was faster in thinner, more porous constructs whilst constructs crosslinked with $BaCl_2$ concentrations of above 10 mM had denser biofilm formation. 3D MRSA and MSSA biofilm constructs were found to show greater resistance to antimicrobials than corresponding two-dimensional (2D) cultures. Thicker 3D *E. coli* biofilms had greater resistance to tetracycline than thinner constructs over 7 d of treatment. Our methodology allowed for the precise 3D bioprinting of self-supporting 3D bacterial biofilm structures that developed biofilms during extended culture. 3D biofilm constructs containing bacterial biofilms produce a model with much greater clinical relevance compared to 2D culture models and we have demonstrated their use in antimicrobial testing.

Introduction

Biofilms can be defined as three dimensional (3D) structured communities of bacterial cells enclosed in a self-produced polymeric matrix, attached to a solid surface or substratum [1]. Bacterial biofilm formation is crucial to establishing chronic infections including respiratory infection [2], orthopaedic infection [3], heart valve infection (endocarditis) [4], and nosocomial infections [5]. In the case of acute infections, bacteria often exist in the planktonic (or free-swimming) state, allowing effective treatment with antimicrobials. However, once a biofilm develops infections are known to be 10–1000 times more resistant to antimicrobial agents, often rendering standard antimicrobial therapy ineffective without more invasive treatment such as surgery [6]. In the United States of America alone, there are 17 million new biofilm-associated bacterial infections that

lead to estimated health care costs of $94 billion and 550 000 deaths each year [7]. According to the World Health Organization (WHO), urgent action is required to avoid a 'post-antibiotic era', in which common infections and minor injuries can once again kill; antimicrobial resistance (AMR) is projected to result in 10 million deaths every year globally by 2050 [8]. Global concern about AMR is compounded by the fact that it has been 30 years since a new class of antibiotics was last introduced [9]. Therefore, increasing importance is being placed on drug screening, and in particular, antimicrobial susceptibility testing (AST), which requires suitable models that more closely resemble *in vivo* biofilm formation.

The minimum inhibitory concentration (MIC) of antimicrobial agents (defined as the lowest concentration of an antimicrobial agent at which visible bacterial growth is inhibited after overnight incubation) is frequently calculated during AST to assess antimicrobial efficacy and bacterial resistance [10]. Methods to determine the MIC based on two-dimensional (2D) planktonic cultures of bacteria are well established [11]. However, determining the minimal biofilm eradicating concentration (MBEC) in biofilm infections is much more challenging. This is primarily because *in vivo* biofilm formation is 3D in architecture, which differs to most currently available laboratory models that tend to involve 2D biofilm culture [12–14]. AST of planktonic bacteria therefore tends to give misleading results that do not reflect the increased resistance of bacteria living in a 3D biofilm [15, 16]. This has significant clinical implications; for example, antimicrobial agents are usually chosen on the basis of their efficacy against 2D planktonic cultures which are more sensitive to treatment than 3D biofilms. Clinically this is well demonstrated by cystic fibrosis patients, where treatment of *P.aeruginosa* infection with antibiotics originally developed against planktonic cultures often becomes ineffective once biofilm formation occurs [15]. To develop novel antimicrobials capable of disrupting biofilm formation and resistance in future, 3D *in vitro* biofilm models more representative of clinical infection are required.

Most commonly used 2D biofilm culture methods attempt to simulate the nature of the *in vivo* environment by focussing on selected relevant factors such as materials, nutrients and, importantly, fluid flow including drip flow [16], rotating disk [17], microfluidics [18], and flow chamber architecture [19]. Unfortunately, none of these methods mimic the complexity of the 3D microenvironment and host defence mechanisms [20] and unable to produce biofilm thicknesses beyond 100 μm [21, 22]. In contrast to the current *in vitro* models, *in vivo* biofilms can grow beyond 1000 μm in size and are often found embedded within a host's extracellular matrix, leading to interactions with the host immune system which can further alter biofilm morphology and size [1, 23].

3D bioprinting has developed rapidly as a technique that can deposit living cells and biomaterials in user-defined patterns to build complex tissue constructs 'from the bottom up' [24–27]. While there are elegant approaches on 3D bioprinting bacteria and their aggregates [28–32], there has been no report on demonstrating the formation of mature bacteria biofilms. However, the capacity to reliably and reproducibly 3D bioprint bacterial biofilms have several potential benefits. Embedded bacteria have been shown to have increased metabolic activity, AMR and plasmid stability compared to bacteria grown in [33, 34]. 3D bioprinted bacterial biofilms therefore could potentially mirror *in vivo* bacterial growth and behaviour more closely than traditional 2D models, increasing the potential to investigate critical bacterial quorum sensing and antimicrobial biofilm penetration [34, 35]. 3D bioprinting also increases the potential to produce biofilm constructs with predesigned dimensions, with a high degree of control possible over biofilm thickness and dimensions. Other benefits of 3D bioprinting biofilm include the potential creation of microbial fuel cells [36], biosensors [37] and biotechnological applications [37–39].

In this paper, we present a novel 3D bioprinting biofilm technology and report the first investigation of the formation of mature bioprinted 3D biofilms and measure their responses to antibiotic drug tests, and drug penetration. Mature biofilms with different thicknesses and structures were designed and bioprinted using a range of clinically relevant bacterial strains. *In vitro* AST was performed to compare the resistance of 2D cultures versus 3D printed biofilm constructs for the first time. Bioprinting of biofilm constructs with thicknesses greater than previously available *in vitro* models was also successfully performed.

Materials and methods

Bacteria-laden bioink preparation

Brain Heart Infusion (BHI) broth (Sigma-Aldrich, UK) powder was dissolved in sterile deionized water to produce a 37 g l^{-1} BHI Broth and then autoclaved. UV-sterilised sodium alginate powder (Protanal LF10/60FT, FMC Biopolymer, UK) was then dissolved in BHI Broth to produce a 4% (w/v) alginate solution. The alginate solution was subjected to magnetic stirring until reaching homogeneity and then sterilised through heating to boiling point (95 °C) three times. Solutions consisting of 4% w/v sodium alginate and 0.4% w/v CaCl$_2$ were then mixed with a volume ratio of 1:1 to create a partially cross-linked 0.2% CaCl$_2$:2% sodium alginate hydrogel in a 50 ml conical tube. The hydrogel solution was vortex mixed at room temperature (RT) at 1500 rpm for 5 min to produce a homogeneous, partially cross-linked alginate hydrogel. Alginate hydrogels were then stored at 4 °C prior to usage to prevent the growth of contaminants.

Bacterial strains and growth media

Bacterial strains were universally cultured in BHI broth at 37 °C whilst shaking. Strains used included *Escherichia coli* (*E. coli* clinical isolate, ATCC 25922), *Pseudomonas aeruginosa* (*P. aeruginosa,* PAO1, wild type strain, ATCC 47085), Methicillin-sensitive *Staphylococcus aureus* (MSSA, clinical isolate, ATCC 29213) and Methicillin-resistant *Staphylococcus aureus* (MRSA, clinical isolate, ATCC 700788). Chosen strains were routinely maintained on BHI agar (Sigma-Aldrich, UK) plates and stocks kept frozen in glycerol (50% v/v) at −80 °C.

Inoculum preparation

Bacterial strains taken from glycerol stocks were streaked on to a BHI agar plate and incubated at 37 °C overnight. The following day a single colony was inoculated into 5 ml of BHI broth and incubated overnight at 37 °C, with 200 rpm shaking (Mini shaker, Cleaver). The overnight cultures were harvested in the stationary phase after 18 h cultivation. The bacteria were collected by centrifugation (3000 rpm, 4 °C, 5 min) and washed three times with 9% sodium chloride (NaCl) to remove the residual BHI medium. In all experiments, the concentration of bacteria was determined by optical density spectrometry (Eppendorf BioPhotometer) and inoculated to 1.0 at wavelength 600 nm ($OD_{600nm} = 1.0$). The inoculated suspension of each strain was prepared in 10 ml of 9% NaCl in a 50 ml centrifuge tube (Fisher Scientific, UK) and the cells harvested by centrifugation (3000 rpm, 4 °C, 5 min). Bacterial cell-pellets were then re-suspended in 500 μl of 0.2% CaCl$_2$:2% sodium alginate hydrogel solution with a *micropipette* and dispensed into a 5 ml Luer-lock syringe (Fisher Scientific, UK). Connection to a further 5 ml Luer-lock syringe containing 4.5 ml 0.2% CaCl$_2$: 2% sodium alginate hydrogel warmed to 37 °C allowed repeated, gentle mixing to be carried out back and forth between syringes containing bacteria and hydrogel (100 mixes back and forth), producing 5 ml bioink with homogeneously distributed bacteria.

Construct design

3D models consisting of a solid or lattice 10 mm × 10 mm square design with increasing vertical thicknesses (0.25, 0.5, 1, 2, 4 mm) were produced using Autodesk® *Netfabb*® software (Autodesk®, Inc., USA) and exported as an STL file. Open-source slicer software (Sli3er, Version 1.2.9) was used to load the STL files and generate G-code files using the following settings for bioprinting: layer thickness, 0.1 mm; infill pattern, rectilinear; infill density, 25%; speed, 10 mm s^{-1}; extrusion multiplier 1.2. G-code files corresponding to solid and lattice constructs with differing vertical thicknesses were then loaded onto the bioprinter.

Bioprinting

A three-axis (*X–Y–Z*), single nozzle 3D cell printer developed in our laboratory was used for bioprinting bioinks laden with different bacteria. This bioprinter represents an adapted, extrusion-based version of a previously developed microvalve-based bioprinter used in our lab to bioprint human cells including induced pluripotent stem cells [26, 39, 40]. Briefly, the bioprinter produces 3D constructs by coordinating the motion of a mechanically-driven syringe. The dispenser deposits extrudate consisting of hydrogel on a stationary Z-platform. As successive layers of extrudate are deposited, the z-platform moves downwards allowing structures to be bioprinted from the bottom up, layer-by-layer. Prior to use, the bioprinter was sterilized via UV exposure and wiped down with 70% ethanol. Sterility was maintained during bioprinting by placing the bioprinter in a laminar flow cabinet. Sterile 5 ml Luer-lock syringes containing bacterial bioink were attached to 25 G printing nozzles and loaded into the bioprinter, allowing bioprinting into sterile 6-well culture plates to occur.

Secondary cross-linking of constructs

Ethylenediaminetetraacetic acid (EDTA), calcium chloride (CaCl$_2$) and barium chloride (BaCl$_2$) powders (Sigma-Aldrich, UK) were sterilised with ultraviolet (UV) light (three 30 min cycles). Solutions of 0.4% w/v CaCl$_2$, 10 mM BaCl$_2$, 20 mM BaCl$_2$, 40 mM BaCl$_2$ and 110 mM EDTA (Sigma-Aldrich, UK) were prepared in sterile deionised water. All solutions were then autoclaved at 121 °C for 30 min prior to experimental usage.

Following bioprinting, constructs were cross-linked by submersion in ionic solutions of either 10, 20 or 40 mM BaCl$_2$ for 2 min. Cross-linked constructs were then rinsed in phosphate-buffered saline (PBS) prior to incubation in BHI medium under standard culture conditions (37 °C, 5% CO$_2$, and 95% relative humidity). BHI media was replenished every second or third day and culture was performed atop a compact fixed-angle platform rocker (Grant Bio™ PMR-30 Compact Fixed-Angle Platform Rocker, Fisher Scientific, UK), to increase flow of media around the bioprinted constructs.

Fluorescence staining for biofilm viability

A commercial Film Tracer™ LIVE/DEAD™ biofilm viability kit (Thermo Fisher) was used for the assessment of biofilm viability based on staining with the membrane potential sensitive dye propidium iodide (PI) (490 nm excitation, red emission) and the nucleic acid stain SYTO-9 (488 nm excitation, green emission). In principle, bacteria with intact cell membranes stain fluorescent green, whereas bacteria with damaged membranes stain fluorescent red. Cell viability staining of bacteria was carried out by incubating biofilm constructs concomitantly with SYTO-9

(6.7 μM) and PI (40 μM) in 35 mm glass bottomed imaging dishes (Ibidi) at RT for 45 min to allow stain penetration.

Biofilm morphotype analysis

In this study, a Leica Microsystems TCS SP8 CARS microscope utilising a 25× objective (HC FLUOTAR L 25×/0.95 W) was used for all confocal fluorescence imaging measurements. To minimise or eliminate artefacts associated with simultaneous dual wavelength excitation, all dual labelled biofilms were sequentially scanned, frame-by-frame, first at 488 nm (Argon laser, 70 μW) then at 561 nm (DPSS laser, 80 μW). Line averaging (×2) was used to capture images with reduced noise. Fluorescence emission was then sequentially collected in the green and red regions of the spectrum respectively. Images were captured in a 2D projection. For analysing spatial separation in the z-direction (thickness), step sizes between 40 and 140 μm were used and 3D reconstructions were performed using Leica imaging software (LAS X). Five image stacks were (typically 700 × 700 μm images over a depth of 40–140 μm) were acquired randomly from three independent constructs per BaCl$_2$ concentration per time point (15 stacks in total). The image stacks were then analysed using MATLAB 2016A software.

Antibiotic susceptibility testing (AST)

For all AST methods, inocula of the isolate tested were prepared according the inoculum preparation protocol described above.

The methicillin stock solution of 20 mg ml^{-1} was prepared in sterile dH$_2$O and diluted in BHI broth to obtain solutions with preliminary concentration in a range of 2.5–10 mg ml^{-1}. Investigation of the response of 3D biofilm constructs to methicillin was then made by initially culturing porous, 1 mm constructs containing MRSA or MSSA for 14 d to allow biofilm maturation to occur. The matured biofilm constructs were then transferred to sterile Corning™ 6-well microtiter plates (Sigma-Aldrich, UK). A 3 ml volume of each methicillin solution was dispensed into each well of the plate. Fresh BHI broth was then added without antibiotic into the positive control wells. The plates were sealed with an anaerobic film (Thermo Fisher Scientific, UK) and incubated under anaerobic conditions at 37 °C for 24 h.

2D broth microdilution method

Corning 96-well microtiter plates (Sigma-Aldrich, UK) were used for determining the MICs of the antimicrobial agents methicillin sodium salt (Sigma-Aldrich, UK). A methicillin concentration in a range of 0.02–5 mg ml^{-1} were used. The MRSA and MSSA inoculum plural (OD1.0) were prepared as described above. A 50 μl volume of each methicillin solution and a 50 μl of inoculated suspension were dispensed into

each well of the microtiter plates respectively. The 96-well plates were then sealed with an anaerobic film (Thermo Fisher Scientific, UK) and incubated under anaerobic conditions at 37 °C for 24 h. The optical density of inoculated culture wells was then measured using a plate reader (Multiskan Go, Thermo Scientific). Subsequently, MICs were read as the lowest concentration of an antimicrobial agent at which visible growth was inhibited.

3D broth macrodilution method

Methicillin stock solution of 20 mg ml^{-1} was prepared in sterile dH$_2$O and diluted in BHI broth to obtain solutions with preliminary concentrations ranging from 2.5 to 10 mg ml^{-1}. Investigation of the response of 3D biofilm constructs to methicillin was then performed by exposing a series of porous, 1 mm MRSA or MSSA constructs to increasing concentrations of methicillin. MRSA and MSSA constructs were cultured for 14 d prior to methicillin exposure to allow biofilm maturation to occur. Mature MRSA and MSSA biofilm constructs were then transferred into sterile Corning® 6-well plates (Sigma-Aldrich, UK) and incubated in 3 ml volumes of either 2.5, 5 or 10 mg ml^{-1} methicillin solution. Positive-control wells containing fresh BHI broth, no methicillin and MRSA or MSSA constructs were also set up. The 6-well plates were sealed with an anaerobic film (Thermo Fisher Scientific, UK) and incubated under anaerobic conditions at 37 °C for 24 h. The optical density of inoculated culture wells was again measured using a plate reader (Multiskan Go, Thermo Scientific).

Biofilm antimicrobial penetration test

3D bioprinted *E. coli* biofilm constructs of 1 and 2 mm thickness and porous design were cultured for 14 d to allow significant biofilm formation to occur. Biofilm constructs were then washed ×3 with phosphate buffered saline (PBS) solution to remove non-adherent bacteria. Antibiotic disks containing 30 μg tetracycline (Oxoid, UK) were then placed on top of *E. coli* biofilm constructs and incubated at 37 °C for 7 d within BHI broth. The tetracycline disks located on top of the biofilm constructs were replaced daily to maintain consistent delivery of antibiotic.

Results and discussions

Developing long-term stability of bioprinted alginate hydrogels to allow observation of 3D biofilm formation

The schematic presented below (scheme 1) elucidates our general methodology of bacterial biofilm bioprinting using a biocompatible bioink [40, 41], extrusion bioprinting and a step-wise ionic crosslinking process. Cultured bacteria were mixed into a partially-crosslinked hydrogel to produce a bioink with homogenous bacterial concentration. A home-built bioextrusion

Scheme 1. Schematic of bacterial biofilm bioprinting process. Initial designs to be bioprinted were produced using computer-aided design (CAD) software. Following this, a partially cross-linked hydrogel was produced by mixing sodium alginate and calcium chloride (CaCl$_2$) together. Bacteria were then mixed into the hydrogel to produce a bioink with homogenously distributed bacteria. 3D bioprinting was then performed, using a custom-built bioprinter that uses mechanical force to extrude bioink from a syringe that is moved in the x–y–z plane. Bioprinted constructs of solid and porous design were then immersed in solutions of barium chloride (BaCl$_2$) for 2 min to secondary cross-link the constructs. Following bioprinting and immersion cross-linking, the constructs were cultured in bacterial growth media, allowing analysis to be performed at selected time points.

based bioprinter was then used to extrude the bioink to produce constructs with predesigned dimensions. Following bioprinting, secondary ionic cross-linking of the hydrogel was performed to increase construct stability, allowing prolonged culture and observation (up to 28 d).
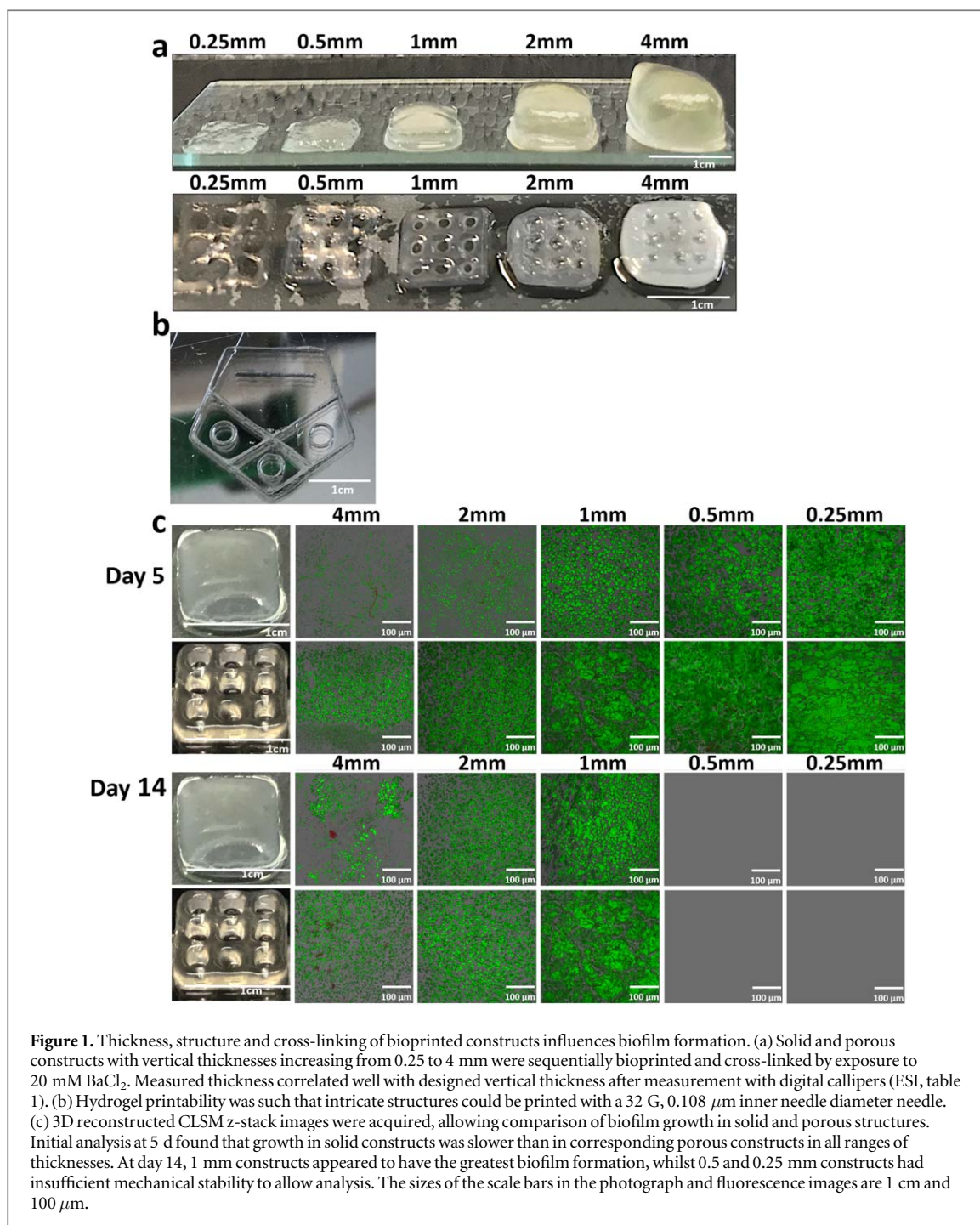
The complex structure of 3D biofilms found in clinical infection take significantly longer to develop and mature than the simpler, 2D biofilm *in vitro* models which can be produced in overnight laboratory culture [3, 42]. Achieving sufficient stability in bioprinted bacterial construct was therefore essential to allow time for bacteria to associate, proliferate and deposit their own extracellular polymeric matrix to form a mature 3D biofilm structure. Alginate is a widely-adopted hydrogel for bioprinting and was chosen as the main component of our bacterial bioink due to its biocompatibility, low toxicity, low cost and ease of use [25, 43, 44].

In previous work we have developed the stability of alginate bioinks to allow the successful long-term 3D cell culture and differentiation of stem cells [25, 44]. This was achieved by double cross-linking alginate with calcium and then barium cations in a stepwise process [44]. We adapted this approach to produce double cross-linked bacterial bioink constructs with extended stability (>4 weeks) in culture. Other cations including strontium have been utilized elsewhere for this purpose; however, barium has been shown to give the strongest cross-linking effect, optimizing construct mechanical stability [45]. Initial cross-linking of sodium alginate hydrogel with calcium chloride created a hydrogel with sufficient viscosity to allow successful bioprinting of free-standing structures of both solid and porous design, ranging in thickness from

0.25 to 4 mm (figure 1(a)). By performing alginate hydrogel cross-linking prior to bioprinting, rather than extruding alginate onto a calcium-coated culture surface as performed in other literature, homogenous hydrogel cross-linking was achieved; this is essential to achieve good printability [28]. Further cross-linking occurred following bioprinting by exposure to solutions of barium chloride which further helped to maintain construct stability, extending the stability of constructs from within a week (with calcium-only cross-linking) to over 4 weeks in culture. (ESI, figures S1 and S2 are available online at stacks.iop.org/BF/11/045018/mmedia.) Bioprinting resolution with the hydrogel was sufficient to produce more intricate structures using a 32 g printing needle, corresponding to a 108 μm inner needle diameter (figure 1(b)).

Confocal laser scanning microscopy (CLSM) was used to observe 3D bioprinted biofilm formation. Standard light microscopes often struggle to image biofilm of more than 3–4 μm thickness as biofilm material above and below the focal plane tend to scatter light and interfere with direct measurement [46]. Contrastingly, CLSM allows optical sectioning of biofilms and, with image analysis, 3D reconstruction is possible [47].

The extended hydrogel stability after bioprinting allows observation of 3D biofilm formation for several weeks. Previous attempts reported elsewhere in the literature to 3D bioprint bacteria only demonstrated bacterial viability up to a maximum of 7–9 d, with no attempts made to perform antimicrobial testing on 3D bioprinted bacterial constructs [28, 30, 31]. The stability in culture of the bioprinted hydrogel-bacteria construct achieved in our study is therefore significant, as it allows for extended observation of bacterial growth

Figure 1. Thickness, structure and cross-linking of bioprinted constructs influences biofilm formation. (a) Solid and porous constructs with vertical thicknesses increasing from 0.25 to 4 mm were sequentially bioprinted and cross-linked by exposure to 20 mM $BaCl_2$. Measured thickness correlated well with designed vertical thickness after measurement with digital callipers (ESI, table 1). (b) Hydrogel printability was such that intricate structures could be printed with a 32 G, 0.108 μm inner needle diameter needle. (c) 3D reconstructed CLSM z-stack images were acquired, allowing comparison of biofilm growth in solid and porous structures. Initial analysis at 5 d found that growth in solid constructs was slower than in corresponding porous constructs in all ranges of thicknesses. At day 14, 1 mm constructs appeared to have the greatest biofilm formation, whilst 0.5 and 0.25 mm constructs had insufficient mechanical stability to allow analysis. The sizes of the scale bars in the photograph and fluorescence images are 1 cm and 100 μm.
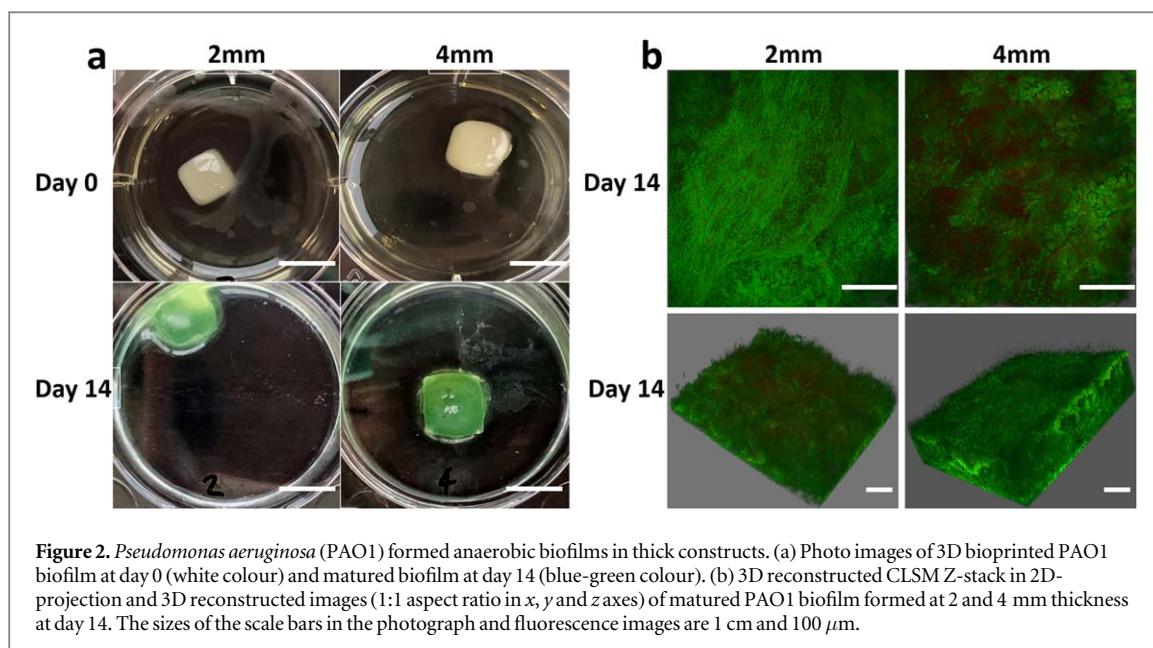
as well as offering the potential to perform antimicrobial studies and further analysis of biofilm formation in 3D. Clinical biofilm infections are most often chronic in nature and develop over a period of weeks and even months; the stability of our bioprinted constructs may therefore facilitate greater potential to mirror clinical biofilms than currently available biofilm models [3, 7, 15, 48, 49].

Investigating the influence of construct design and thickness on biofilm formation

In order to mimic *in vivo* biofilms and to create an ideal *in vitro* 3D bioprinted biofilm model, solid and porous constructs were bioprinted in a range of thicknesses from 0.25 to 4 mm to investigate the ideal construct design and thickness for *E. coli* biofilm formation.

E. coli biofilm formation (or bacterial density) was greater in thinner (0.25–1 mm), constructs compared to thicker (4 mm) construct designs ($p < 0.001$, ANOVA) (figure 1(c)). However, thinner constructs of 0.25 and 0.5 mm thickness were not robust enough to allow physical manipulation and CLSM imaging to be performed after 14 d culture. This was presumed to be due to leaching of cations (Ca^{2+} and Ba^{2+}) from the thin, relatively high-surface area constructs into surrounding culture media, resulting in decreased cross-linking; this is likely to have been exacerbated by

Figure 2. *Pseudomonas aeruginosa* (PAO1) formed anaerobic biofilms in thick constructs. (a) Photo images of 3D bioprinted PAO1 biofilm at day 0 (white colour) and matured biofilm at day 14 (blue-green colour). (b) 3D reconstructed CLSM Z-stack in 2D-projection and 3D reconstructed images (1:1 aspect ratio in *x*, *y* and *z* axes) of matured PAO1 biofilm formed at 2 and 4 mm thickness at day 14. The sizes of the scale bars in the photograph and fluorescence images are 1 cm and 100 μm.

regular media changes and culture atop a rocking device, increasing outwards diffusion of cations from the hydrogel-bacteria construct. In 4 mm thick constructs, reduced biofilm formation was observed in solid compared to porous constructs ($p = 0.038$, t-test) (figure 1(c)).

We believe the porous construct design facilitates convective fluid transport through the pore channels, enhancing nutrient and oxygen diffusion processes in comparison to non-porous, solid constructs. This would explain why the aerobic bacteria *E. coli* failed to proliferate and produce significant biofilm in the thick, solid constructs, with the optimal structure for *E. coli* being a 1 mm porous construct.

Bioprinting of thick, anaerobic 3D biofilm constructs

Whilst the aerobic bacteria *E. coli* had limited growth in thicker bioprinted constructs (figure 1(c)), presumably due to limited diffusion of nutrients and oxygen, anaerobic bacteria have greater potential to thrive in oxygen-deplete conditions. As an opportunistic, nosocomial pathogen of immunocompromised individuals, the anaerobic strain *Pseudomonas aeruginosa* (*P. aeruginosa*) is well known for infecting the thick, oxygen-depleted mucus in the airways of cystic fibrosis (CF) patients, producing robust *in vivo* biofilms [2]. The culture conditions provided by the thick respiratory mucus in CF patients is somewhat analogous to those provided by our thick, non-porous hydrogel constructs. To investigate this, *in vitro* biofilm formation of *P. aeruginosa* (figure 2) was examined in nonporous, thick (2 and 4 mm) constructs (figure 2).

P. aeruginosa was observed to undergo extensive colonisation and aggregation in 2 mm and 4 mm thick, non-porous structures, forming an extremely dense layer of biofilm (figure 2(b)). In contrast, much more limited bacterial growth and biofilm formation

was observed via CLSM in 2 and 4 mm constructs inoculated with the aerobic bacteria *E. coli* (figure 1(c)). Strong blue-green pigmentation was also seen to form in 2 and 4 mm *P. aeruginosa* constructs over 14 d of culture (figure 2(a)); this is likely related to the expression of two metabolites, pyocyanin (blue) and pyoverdine (green), which is known to occur in *P. aeruginosa* to facilitate anaerobic respiration [50]. The prevalence of multidrug-resistant anaerobes, including *P. aeruginosa*, is increasing worldwide with limited current therapeutic options [51, 52]. The extensive growth of *P. aeruginosa* and associated biofilm formation seen within our 3D bioprinted constructs therefore offers a novel and highly promising *in vitro* method of studying anaerobic bacterial biofilm infection.

Capturing the *in vitro* life cycle of biofilm in 3D

Biofilm formation is reported to occur in a five-step lifecycle (figure 3(a)), which begins with the attachment of planktonic cells to a biological or inert surface and culminates in mature biofilm formation [53]. However, due to factors including limited biofilm thickness, current *in vitro* models are unable to readily facilitate observation of the five-step process and complex microarchitecture development that occurs during biofilm formation [54].

As illustrated in figure 3(a), Initially, ① free swimming planktonic bacteria were attached on the surface, ② Soon after, bacteria began to divide and aggregate together in small microcolonies and secrete quorum signals ③, which initiated up-regulation of various genes and virulence factors on a community-wide basis. Bacteria cells forming an extracellular biofilm matrix ④ by secrete copious polymers including polysaccharides, proteins and oligonucleotides. Biofilm continues to accumulate and consuming ambient nutrient and QC acceptors. As results of increased in
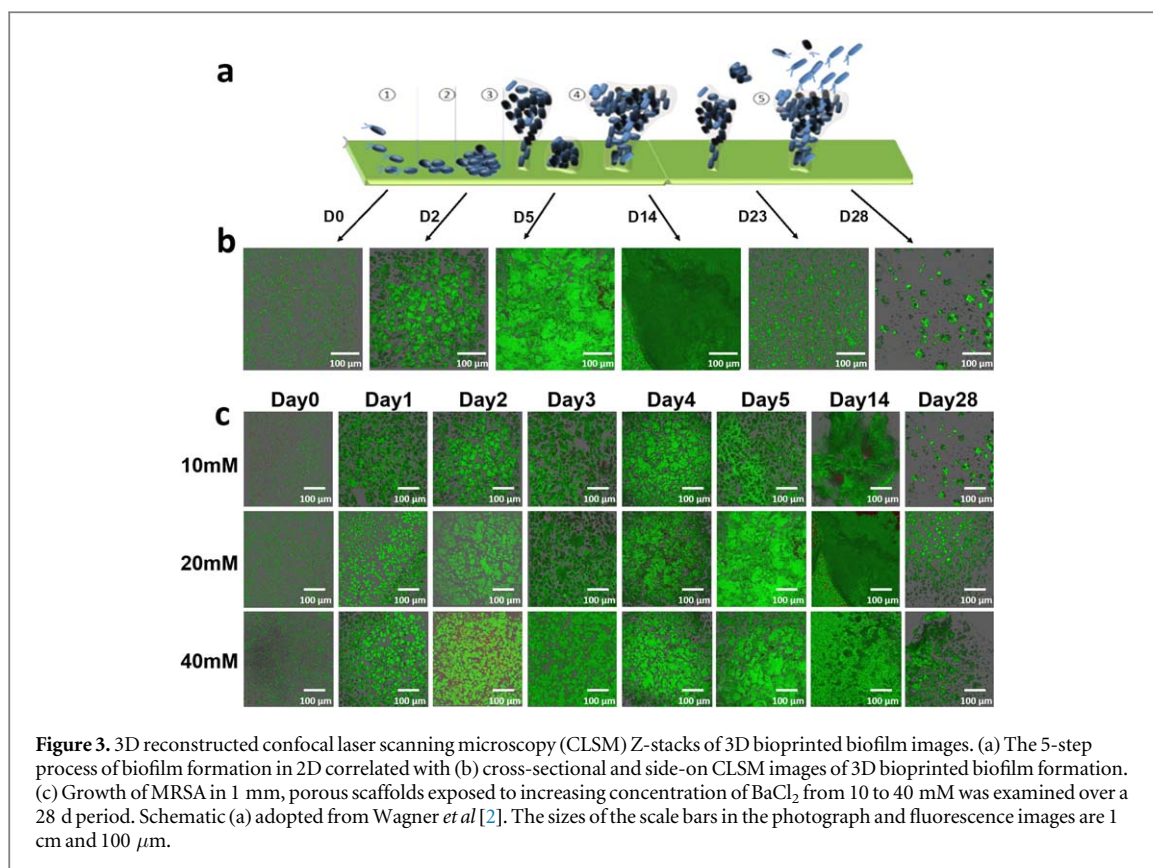
Figure 3. 3D reconstructed confocal laser scanning microscopy (CLSM) Z-stacks of 3D bioprinted biofilm images. (a) The 5-step process of biofilm formation in 2D correlated with (b) cross-sectional and side-on CLSM images of 3D bioprinted biofilm formation. (c) Growth of MRSA in 1 mm, porous scaffolds exposed to increasing concentration of $BaCl_2$ from 10 to 40 mM was examined over a 28 d period. Schematic (a) adopted from Wagner *et al* [2]. The sizes of the scale bars in the photograph and fluorescence images are 1 cm and 100 μm.

shear stress and other cell signalling events, portions of biofilm started detaching or slough off ⑤ entirely. Dispersed cells can quickly revert to their planktonic form to colonise other sites, whilst retaining properties such as AMR [54].

The influence of $BaCl_2$ cross-linking concentration on bacterial growth was also analysed over 28 d by exposing porous, 1 mm constructs containing MRSA to a range of $BaCl_2$ concentrations (ESI, figure S3). Growth within all constructs was initially strong; however, it was perceptible that bacteria had a greater tendency to leach from constructs exposed to 10 mM $BaCl_2$, with greater biofilm formation seen in 20 and 40 mM constructs (figure 3(c)). A custom designed image processing algorithm, implemented in MATLAB 2016a, was used to apply further statistical analysis to quantify biofilm formation (ESI, figures S4 and S5). It was found that 10 mM of $BaCl_2$ provided less favourable conditions for biofilm formation compared to 20 and 40 mM constructs between days four and 23 ($p < 0.001$, ANOVA). This was presumed due to reduced cation (Ba^{2+}) cross-linking density allowing greater leaching of bacteria.

CLSM studies demonstrated superior biofilm formation in 10, 20 and 40 mM constructs, with significant biofilm formation evident after 5 d. Initially, ① individual planktonic bacteria were homogenously distributed in bioink at day 0 (figure 3(c), day 0). Although some bacteria may have left the construct, a high density remained and likely adhered to the bioink scaffold using cell surface displayed adhesin

molecules. ② Soon after, bacteria began to divide and aggregate together in small microcolonies (figure 3(c), day 1–2) with in the construct, which merged into larger communities (figure 3(c), day 3–5); ③ progressive deposition of an EPS matrix also occurred, ④ leading to mature biofilm formation (figure 3(c), day 14). Eventually, ⑤ regions of biofilm were seen to spontaneously disperse between days 23 and 28 as bacteria enzymatically dissolved the extracellular matrix [55], weaken the biofilm structure and release microbial cells spread and leak out of the construct (figure 3(c), day 23–28) into surrounding culture media (where new biofilms can be formed). It is important to observe that 3D bioprinted alginate constructs remains largely intact while the bacteria escaped from constructs (ESI, figure S2) after day 23. This further confirms that the lower microbial cell density observed from day 23–28 was consistent with the final stage of the biofilm lifecycle where bacteria leak out of the biofilm and spread rather than the degradation of the 3D alginate constructs.

To the best of our knowledge, we have demonstrated for the first time the processes involved in mature 3D biofilm formation *in vitro* over a 28 d period using bioprinting (figure 3(c)). This allows direct correlation to the 5-step process governing biofilm formation in 2D to be made (figure 3(a)).

Comparison of 2D versus 3D *in vitro* AST

To compare the susceptibility of 2D and 3D bacterial cultures to treatment, we utilised 3D bioprinted

biofilms as an *in vitro* model with comparison made to 2D bacterial cultures. *Staphylococcus aureus* (*S. aureus*) was chosen for investigation as a major human pathogen[56]. Although most commonly associated with skin and soft tissue infections, *S. aureus* is also responsible for a range of serious invasive infections, including osteomyelitis, necrotising pneumonia, endocarditis and bacteraemia [56]. Infections caused by *S. aureus* are increasing worldwide, with over 52% of intensive care unit infections reported to be caused by *S. aureus* [57]. Most strains of *S. aureus*, including methicillin-susceptible *S. aureus* (MSSA), are sensitive to β-lactam antibiotics and are responsive to treatment. However, there is a growing worldwide prevalence of methicillin resistant *S. aureus* (MRSA) infections, which have repeatedly been associated with a worse patient outcome compared to infections caused by methicillin sensitive *S. aureus* (MSSA) [58]. Furthermore, the efficacy of first-line treatments for MRSA such as vancomycin is dwindling [59]. Antibiotic resistance studies are therefore essential to allow the development of novel anti-biofilm therapies against MRSA and MSSA biofilms.

The broth microdilution method was used to determine the lowest concentration (MIC) of methicillin antibiotic that prevented visible growth of MRSA and MSSA in 2D culture (figure 4(a)). The broth macrodilution method was then used to determine the MBEC in 3D bioprinted MRSA and MSSA biofilm culture models (figure 4(c)). The MIC and MBEC were determined by a visual inspection of culture wells and correlated with measurements of absorbance of light through treated culture wells in both cases (figures 4(b) and (d)). Due to resistance to methicillin, MRSA had a higher MIC than MSSA in 2D (figure 4(a)) and a higher MBEC than MSSA in 3D culture as expected (figure 4(c)). However, for both MRSA and MSSA, the MBEC calculated in 3D culture was significantly higher than the MIC for 2D culture. Whilst 0.16 μg ml^{-1} methicillin prevented visible growth of 2D MSSA culture, the MBEC for MSSA in 3D culture appeared to be at least 15 times higher at 2.5 mg ml^{-1}. Similarly, although 1.25 μg ml^{-1} methicillin appeared to prevent 2D growth of MRSA, growth of MRSA in 3D culture still occurred with greater than 10 mg ml^{-1} methicillin. Therefore, for both MRSA and MSSA, a far higher dose of methicillin was required to treat biofilm growth than was required to treat 2D infection. This result is in keeping with previous reports suggesting that biofilm formation can cause a 10–1000 fold increase in bacterial tolerance to antimicrobial treatment compared to 2D, planktonic cultures [33, 55].

Biofilm thickness influences response to treatment
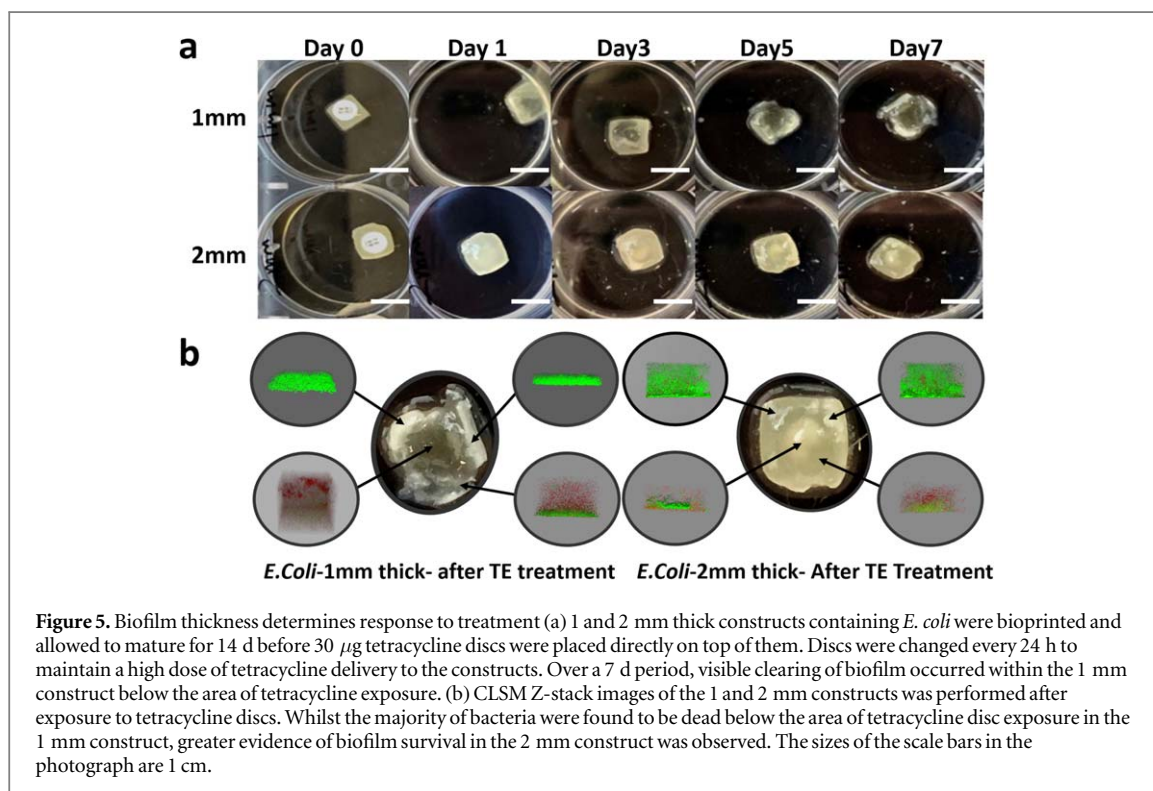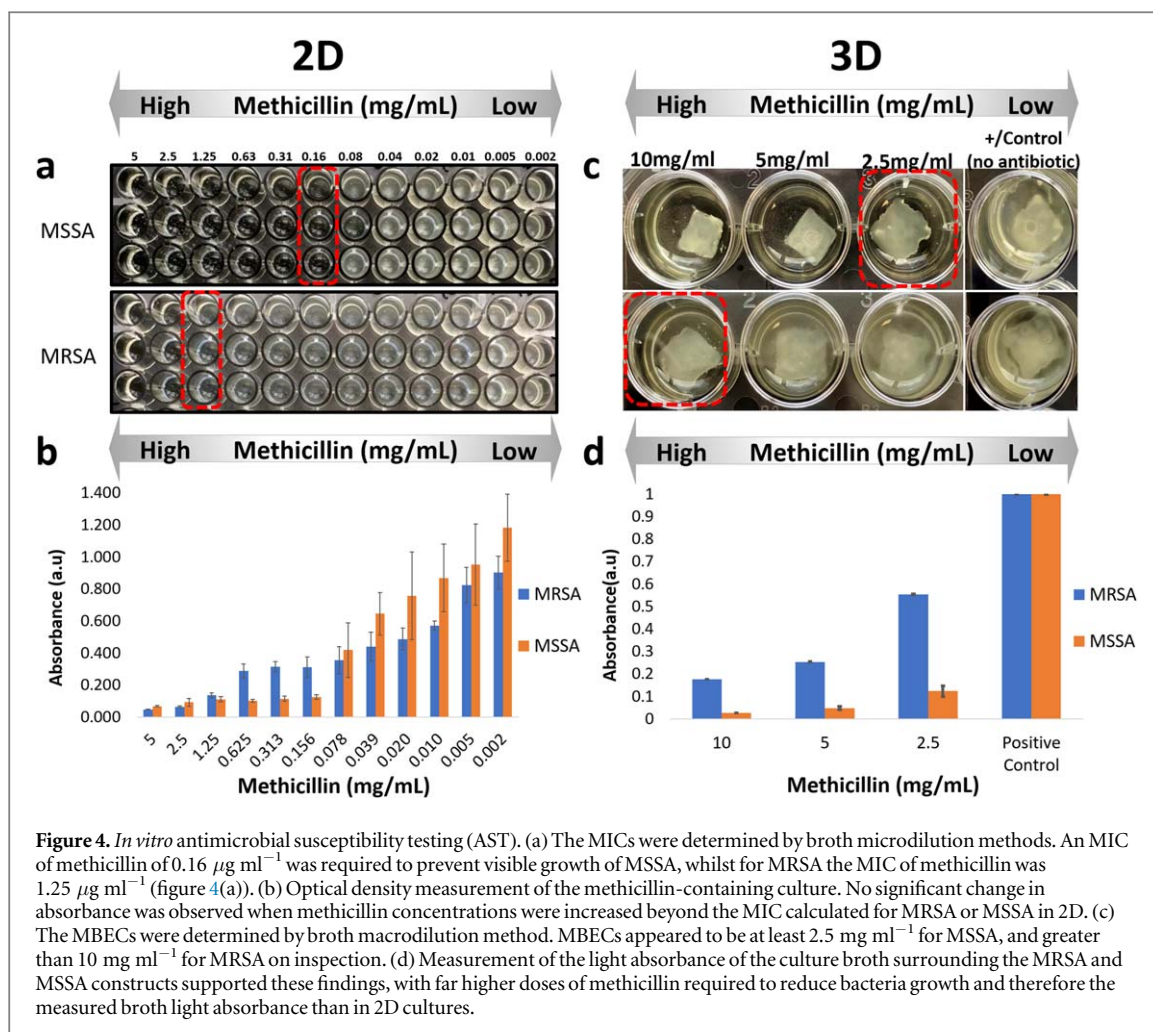AST methods such as MIC calculation do not distinguish between bactericidal and bacteriostatic effects of antibiotoics, and crucially do not provide information on the degree of antimicrobial biofilm penetration or eradicaiton [1, 4, 13, 20, 21, 50, 60, 61]. Utilising 3D bioprinted biofilms as an *in vitro* model, we sought to investigate the relationship between bacterial biofilm thickness and susceptibility to antimicrobial treatment. Sensitivity of *E. coli* to tetracycline was first confirmed in 2D culture (ESI, figure S6). Bioprinted *E. coli* constructs of 1 and 2 mm thickness were then grown for 14 d to allow biofilm maturation, before exposure to 30 μg tetracycline discs which were changed every 24 h for 7 d, mimicking a course of clinical antimicrobial treatment (figure 5(a)). It was apparent that 2 mm constructs remained opaque whilst 1 mm constructs became increasingly transparent in response to tetracycline exposure (figure 5(a)). CLSM imaging of the constructs after 7 d of tetracycline exposure demonstrated that *E. coli* biofilms had greater viability in 2 mm constructs, whilst bacteria located below the tetracycline disc in 1 mm constructs had largely been destroyed (figure 5(b)).

As discussed previously, current methods of studying antimicrobial biofilm penetration and eradication suffer significant limitations. However, 3D bioprinted biofilms could offer hope for a novel and reproducible method of studying antimicrobial biofilm penetration and eradication in 3D. In the clinical environment 3D bioprinted biofilms could feasibly be generated from bacterial samples taken from patients in a similar manner to our experiment; this would allow antimicrobials to be selected on the basis of their ability to achieve biofilm penetration and eradication in patient-specific infections. Furthermore, it is recognised that 3D cultures (such as our 3D bioprinted biofilm) more closely resemble the *in vivo* biofilm, when compared to traditionally used 2D *in vitro* cultures [12, 13, 15, 16].

Conclusions

In conclusion, mature bacterial biofilm constructs were reproducibly 3D bioprinted for the first time using clinically relevant bacteria. By deploying a methodology originally developed to enable 3D culture and differentiation of bioprinted stem cells [25], we have been able to demonstrate for the first time 3D bioprinted mature biofilm formation, dispersal and morphology over 28 d, as well as the antibiotic tolerance of clinically relevant bacterial biofilms in 3D. Our methodology also significantly prolongs the viability of bacteria cultured in 3D bioprinted constructs compared to previous studies. Future ability to investigate clinically relevant bacterial biofilms in a biocompatible, cost-effective 3D model that more closely resembles *in vivo* conditions than traditional 2D culture methods is therefore increased.

A high degree of control was achieved over biofilm construct thickness and design, with the production of biofilms thicker (>4 mm) than currently available

Figure 4. *In vitro* antimicrobial susceptibility testing (AST). (a) The MICs were determined by broth microdilution methods. An MIC of methicillin of 0.16 μg ml^{-1} was required to prevent visible growth of MSSA, whilst for MRSA the MIC of methicillin was 1.25 μg ml^{-1} (figure 4(a)). (b) Optical density measurement of the methicillin-containing culture. No significant change in absorbance was observed when methicillin concentrations were increased beyond the MIC calculated for MRSA or MSSA in 2D. (c) The MBECs were determined by broth macrodilution method. MBECs appeared to be at least 2.5 mg ml^{-1} for MSSA, and greater than 10 mg ml^{-1} for MRSA on inspection. (d) Measurement of the light absorbance of the culture broth surrounding the MRSA and MSSA constructs supported these findings, with far higher doses of methicillin required to reduce bacteria growth and therefore the measured broth light absorbance than in 2D cultures.

Figure 5. Biofilm thickness determines response to treatment (a) 1 and 2 mm thick constructs containing *E. coli* were bioprinted and allowed to mature for 14 d before 30 μg tetracycline discs were placed directly on top of them. Discs were changed every 24 h to maintain a high dose of tetracycline delivery to the constructs. Over a 7 d period, visible clearing of biofilm occurred within the 1 mm construct below the area of tetracycline exposure. (b) CLSM Z-stack images of the 1 and 2 mm constructs was performed after exposure to tetracycline discs. Whilst the majority of bacteria were found to be dead below the area of tetracycline disc exposure in the 1 mm construct, greater evidence of biofilm survival in the 2 mm construct was observed. The sizes of the scale bars in the photograph are 1 cm.

in vitro models also achieved. We observed that anaerobic bacteria continued to thrive in constructs of greater than 4 mm thickness, demonstrating the potency of these infections. To our best knowledge, the 4 mm thick aerobic bacteria biofilm formation is the thickest 3D bioprinted *in vitro* biofilm construct ever reported, allowing easy observation of antimicrobial biofilm penetration.

We observed that 3D biofilm constructs had greater resistance to antimicrobial treatment than 2D cultures, underlining the significance of biofilm formation in clinical infection. Thicker biofilms were also seen to have greater resistance to antimicrobial therapy than thinner biofilms, even over a prolonged period of treatment.

With rising worldwide AMR, 3D bioprinted biofilm technology could become a key weapon to aid the discovery of novel therapeutic targets and increase the understanding of biofilm formation.

Acknowledgments

ORCID iDs

Wenmiao Shu   https://orcid.org/0000-0002-1220-361X

References

[1] Bjarnsholt T 2013 The role of bacterial biofilms in chronic infections *Apmis* **121** 1–58
[2] Wagner V E and Iglewski B H 2008 *P. aeruginosa* biofilms in CF infection *Clin. Rev. Allergy Immunol.* **35** 124–34
[3] Zimmerli W and Sendi P 2017 Orthopaedic biofilm infections *Apmis* **125** 353–64
[4] Donlan R M 2001 Biofilm formation: a clinically relevant microbiological process *Clin. Infectious Dis.* **33** 1387–92
[5] Costerton J W, Stewart P S and Greenberg E P 1999 Bacterial biofilms: a common cause of persistent infections *Science* **284** 1318–22
[6] Olsen I 2015 Biofilm-specific antibiotic tolerance and resistance *Eur. J. Clin. Microbiol. Infectious Dis.* **34** 877–86
[7] Wolcott R D, Rhoads D D, Bennett M E, Wolcott B M, Gogokhia L, Costerton J W and Dowd S E 2010 Chronic wounds and the medical biofilm paradigm *J. Wound Care* **19** 45–53
[8] Willyard C 2017 Drug-resistant bacteria ranked *Nature* **543** 15–15
[9] Rolain J M, Abat C, Jimeno M T, Fournier P E and Raoult D 2016 Do we need new antibiotics? *Clin. Microbiol. Infection* **22** 408–15
[10] Luber P, Bartelt E, Genschow E, Wagner J and Hahn H 2003 Comparison of broth microdilution, E test, and agar dilution methods for antibiotic susceptibility testing of *Campylobacter jejuni* and *Campylobacter coli J. Clin. Microbiol.* **41** 1062–8
[11] Jorgensen J H and Ferraro M J 2009 Antimicrobial susceptibility testing: a review of general principles and contemporary practices *Clin. Infectious Dis.* **49** 1749–55
[12] McBain A J 2009 Chapter 4 *in vitro* biofilm models: an overview *Adv. Appl. Microbiol.* **69** 99–132
[13] Hoiby N, Bjarnsholt T, Givskov M, Molin S and Ciofu O 2010 Antibiotic resistance of bacterial biofilms *Int. J. Antimicrob. Agents* **35** 322–32
[14] Macia M D, Rojo-Molinero E and Oliver A 2014 Antimicrobial susceptibility testing in biofilm-growing bacteria *Clin. Microbiol. Infection* **20** 981–90
[15] Tam V H, Chang K T, Abdelraouf K, Brioso C G, Ameka M, McCaskey L A, Weston J S, Caeiro J P and Garey K W 2010 Prevalence, resistance mechanisms, and susceptibility of multidrug-resistant bloodstream isolates of *Pseudomonas aeruginosa Antimicrob. Agents Chemother.* **54** 1160–4
[16] Goeres D M, Hamilton M A, Beck N A, Buckingham-Meyer K, Hilyard J D, Loetterle L R, Lorenz L A, Walker D K and Stewart P S 2009 A method for growing a biofilm under low shear at the air–liquid interface using the drip flow biofilm reactor *Nat. Protocols* **4** 783–8
[17] Hentzer M, Teitzel G M, Balzer G J, Heydorn A, Molin S, Givskov M and Parsek M R 2001 Alginate overproduction affects *Pseudomonas aeruginosa* biofilm structure and function *J. Bacteriol.* **183** 5395–401
[18] Lee J H, Kaplan J B and Lee W Y 2008 Microfluidic devices for studying growth and detachment of *Staphylococcus epidermidis* biofilms *Biomed. Microdevices* **10** 489–98
[19] Pamp S J, Sternberg C and Tolker-Nielsen T 2009 Insight into the microbial multicellular lifestyle via flow-cell technology and confocal microscopy *Cytometry* A **75A** 90–103
[20] Coenye T and Nelis H J 2010 *In vitro* and *in vivo* model systems to study microbial biofilm formation *J. Microbiol. Methods* **83** 89–105
[21] Bjarnsholt T, Alhede M, Alhede M, Eickhardt-Sorensen S R, Moser C, Kuhl M, Jensen P O and Hoiby N 2013 The *in vivo* biofilm *Trends Microbiol.* **21** 466–74
[22] Roberts A E L, Kragh K N, Bjarnsholt T and Diggle S P 2015 The limitations of *in vitro* experimentation in understanding biofilms and chronic infection *J. Mol. Biol.* **427** 3646–61
[23] Moroni L *et al* 2018 Biofabrication: a guide to technology and terminology *Trends Biotechnol.* **36** 384–402
[24] Turnbull G, Clarke J, Picard F, Riches P, Jia L, Han F, Li B and Shu W 2018 3D bioactive composite scaffolds for bone tissue engineering *Bioactive Mater.* **3** 278–314
[25] Faulkner-Jones A, Fyfe C, Cornelissen D J, Gardner J, King J, Courtney A and Shu W M 2015 Bioprinting of human pluripotent stem cells and their directed differentiation into hepatocyte-like cells for the generation of mini-livers in 3D *Biofabrication* **7** 044102
[26] Groll J *et al* 2016 Biofabrication: reappraising the definition of an evolving field *Biofabrication* **8** 013001
[27] Holmes A M, Charlton A, Derby B, Ewart L, Scott A and Shu W M 2017 Rising to the challenge: applying biofabrication approaches for better drug and chemical product development *Biofabrication* **9** 033001
[28] Schaffner M, Ruhs P A, Coulter F, Kilcher S and Studart A R 2017 3D printing of bacteria into functional complex materials *Sci. Adv.* **3** 1–9
[29] Lehner B A E, Schmieden D T and Meyer A S 2017 A straightforward approach for 3D bacterial printing *ACS Synth. Biol.* **6** 1124–30
[30] Huang Y J, Xia A G, Yang G and Jin F 2018 Bioprinting living biofilms through optogenetic manipulation *ACS Synth. Biol.* **7** 1195–200
[31] Schmieden D T, Vazquez S J B, Sanguesa H, van der Does M, Idema T and Meyer A S 2018 Printing of patterned, engineered *E. coil* biofilms with a low-cost 3D printer *ACS Synth. Biol.* **7** 1328–37

[32] Connell J L, Ritschdorff E T, Whiteley M and Shear J B 2013 3D printing of microscopic bacterial communities *Proc. Natl Acad. Sci.* **110** 18380–5

[33] Wu H, Moser C, Wang H-Z, Hoiby N and Song Z-J 2015 Strategies for combating bacterial biofilm infections *Int. J. Oral Sci.* **7** 1–7

[34] Kyle S 2018 3D printing of bacteria: the next frontier in biofabrication *Trends Biotechnol.* **36** 340–1

[35] Boyle K E, Heilmann S, van Ditmarsch D and Xavier J B 2013 Exploiting social evolution in biofilms *Curr. Opin. Microbiol.* **16** 207–12

[36] Logan B E, Hamelers B, Rozendal R A, Schrorder U, Keller J, Freguia S, Aelterman P, Verstraete W and Rabaey K 2006 Microbial fuel cells: methodology and technology *Environ. Sci. Technol.* **40** 5181–92

[37] Dolatabadi S and Manjulakumari D 2012 Microbial biosensors and bioelectronics *Res. J. Biotechnol.* **7** 102–8https://www. researchgate.net/profile/Somayeh_Dolatabadi/publication/ 230739386_Microbial_Biosensors_and_Bioelectronics/links/ 09e41503c7c93c1dde000000/Microbial-Biosensors-and-Bioelectronics.pdf

[38] Cassidy M B, Lee H and Trevors J T 1996 Environmental applications of immobilized microbial cells: a review *J. Ind. Microbiol.* **16** 79–101

[39] Faulkner-Jones A, Greenhough S, King J A, Gardner J, Courtney A and Shu W M 2013 Development of a valve-based cell printer for the formation of human embryonic stem cell spheroid aggregates *Biofabrication* **5** 015013

[40] Li C *et al* 2015 Rapid formation of a supramolecular polypeptide-DNA hydrogel for *in situ* three-dimensional multilayer bioprinting *Angew. Chem.-Int. Ed.* **54** 3957–61

[41] Groll J *et al* 2019 A definition of bioinks and their distinction from biomaterial *Biofabrication* **11** 013001

[42] Azeredo J *et al* 2017 Critical review on biofilm methods *Crit. Rev. Microbiol.* **43** 313–51

[43] Bidarra S J, Barrias C C and Granja P L 2014 Injectable alginate hydrogels for cell delivery in tissue engineering *Acta Biomater.* **10** 1646–62

[44] Tabriz A G, Hermida M A, Leslie N R and Shu W 2015 Three-dimensional bioprinting of complex cell laden alginate hydrogel structures *Biofabrication* **7** 045012

[45] Morch Y A, Donati I, Strand B L and Skjak-Braek G 2006 Effect of Ca^{2+}, Ba^{2+}, and Sr^{2+} on alginate microbeads *Biomacromolecules* **7** 1471–80

[46] Caldwell D E, Korber D R and Lawrence J R 1992 Imaging of bacterial-cells by fluorescence exclusion using scanning confocal laser microscopy *J. Microbiol. Methods* **15** 249–61

[47] Schlafer S and Meyer R L 2017 Confocal microscopy imaging of the biofilm matrix *J. Microbiol. Methods* **138** 50–9

[48] Rasmussen R V, Fowler V G, Skov R and Bruun N E 2011 Future challenges and treatment of *Staphylococcus aureus* bacteremia with emphasis on MRSA (vol 6, pg 43, 2011) *Future Microbiol.* **6** 250

[49] Cosgrove S E, Sakoulas G, Perencevich E N, Schwaber M J, Karchmer A W and Carmeli Y 2003 Comparison of mortality associated with methicillin-resistant and methicillin-susceptible *Staphylococcus aureus* bacteremia: a meta-analysis *Clin. Infectious Dis.* **36** 53–9

[50] Bryers J D 2008 Medical biofilms *Biotechnol. Bioeng.* **100** 1–18

[51] Patrie S M and Mrksich M 2007 Self-assembled monolayers for MALDI-TOF mass spectrometry for immunoassays of human protein antigens *Anal. Chem.* **79** 5878–87

[52] Jamar W, Al Hashem G and Rotimi V O 2015 Antimicrobial resistance among anaerobes isolated from clinical specimens in Kuwait hospitals: comparative analysis of 11-year data *Anaerobe* **31** 25–30

[53] Garnett J A and Matthews S 2012 Interactions in bacterial biofilm development: a structural perspective *Curr. Protein Peptide Sci.* **13** 739–55

[54] Magana M, Sereti C, Ioannidis A, Mitchell C A, Ball A R, Magiorkinis E, Chatzipanagiotou S, Hamblin M R, Hadjifrangiskou M and Tegos G P 2018 Options and limitations in clinical investigation of bacterial biofilms *Clin. Microbiol. Rev.* **31** 4–16

[55] Baselga R, Albizu I and Amorena B 1994 Staphylococcus-aureus capsule and slime as virulence factors in ruminant mastitis-a review *Veterinary Microbiol.* **39** 195–204

[56] Spoering A L and Lewis K 2001 Biofilms and planktonic cells of Pseudomonas aeruginosa have similar resistance to killing by antimicrobials *J. Bacteriol.* **183** 6746–51

[57] Wang H, Hong W, Oana C, Song Z and Hoiby N 2011 Pharmacokinetics/pharmacodynamics of colistin and imipenem on mucoid and nonmucoid pseudomonas aeruginosa biofilms *Antimicrob. Agents Chemother.* **55** 4469–74

[58] Williamson D A, Lim A, Thomas M G, Baker M G, Roberts S A, Fraser J D and Ritchie S R 2013 Incidence, trends and demographics of *Staphylococcus aureus* infections in Auckland, New Zealand, 2001–2011 *BMC Infectious Dis.* **13** 1–9

[59] System N 2002 National Nosocomial Infections Surveillance (NNIS) System Report, data summary from January 1992 to June 2002, issued August 2002 *Am. J. Infection Control* **30** 458–75

[60] Anderl J N, Franklin M J and Stewart P S 2000 Role of antibiotic penetration limitation in Klebsiella pneumoniae biofilm resistance to ampicillin and ciprofloxacin *Antimicrob. Agents Chemother.* **44** 1818–24

[61] Bodelón G *et al* 2016 Detection and imaging of quorum sensing in Pseudomonas aeruginosa biofilm communities by surface-enhanced resonance Raman scattering *Nat. Mater.* **15** 1203